ACS OMEGA

Open Access

http://pubs.acs.org/journal/acsodf

Article

Efficient Fabrication of Self-Assembled Polylactic Acid Colloidosomes for Pesticide Encapsulation

Zulipiker Payizila, Fuquan Teng, Xudong Huang, Wenbiao Liu, Tengfei Wu, Qian Sun,* and Shuangliang Zhao

Cite This: *ACS Omega* 2024, 9, 3781−3792

Read Online

ACCESS | Metrics & More | Article Recommendations | Supporting Information

ABSTRACT: Colloidosomes are microcapsules whose shells are composed of cumulated or fused colloidal particles. When colloidosomes are used for in situ encapsulation, it is still a challenge to achieve a high encapsulation efficiency and controllable release by an effective fabrication method. Herein, we present a highly efficient route for the large-scale preparation of colloidosomes. The biodegradable polylactic acid (PLA) nanoparticles (NPs) as shell materials can be synthesized using an antisolvent precipitation method, and the possible formation mechanism was given through the molecular dynamics (MD) simulation. The theoretical values are basically consistent with the experimental results. Through the use of the modified and unmodified PLA NPs, the colloidosomes with controllable shell porosities can be easily constructed using spray drying technology. We also investigate the mechanism of colloidosomes successfully self-assembled by PLA NPs with various factors of inlet temperature, feed rate, and flow rates of compressed air. Furthermore, avermectin (AVM) was used as a model for in situ encapsulation and a controllable release. The spherical modified colloidosomes encapsulating AVM not only achieve a small mean diameter of 1.57 μm but also realize a high encapsulation efficiency of 89.7% and impermeability, which can be further verified by the MD simulation. AVM molecules gather around and clog the shell pores during the evaporation of water molecules. More importantly, the PLA colloidosomes also reveal excellent UV-shielding properties, which can protect AVM from photodegradation.

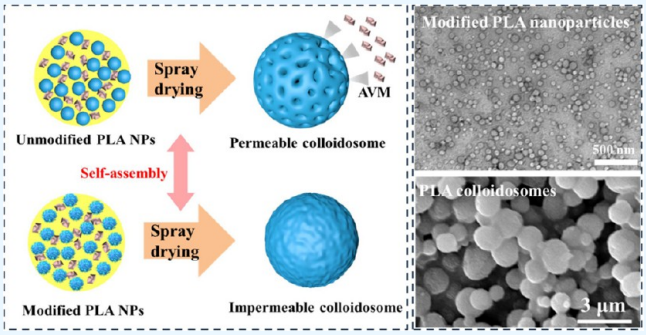

1. INTRODUCTION

Microcapsules are microcontainers with polymer or inorganic shells, which can be used to protect core materials from some harsh denaturing environments.[1] Their potential applications are involved in various fields, such as cosmetics, food, agriculture, and pharmaceutical industries.[2−6] Importantly, for active ingredients that are easy to oxidize, volatilize, and hydrolyze, and pesticides that are easy to photodegrade, the encapsulation process using functional microcapsules can increase their stability and liveness.[7,8] There are a large number of microcapsule preparation methods, such as interfacial polymerization,[9] in situ polymerization,[10] solvent evaporation,[11] layer-by-layer polyelectrolyte deposition,[12] and polymer precipitation by phase separation method.[13] These traditional microcapsule preparation methods normally include the use of massive organic solvents and a relatively complex preparation process, which may have a negative impact on the properties of encapsulated materials, especially for active ingredients.

In order to solve the above issues, the formation of colloidosomes has been widely developed and attracted great attention in the last few decades. Colloidosomes are Pickering emulsion microcapsules whose shells consist of fused polymers or colloidal particles.[14,15] The concept of colloidosomes was first proposed by Velev et al.[16,17] They used polystyrene NPs as shell materials and fixed them on the surface of Pickering emulsion droplets to form stable self-assembled colloidosomes. This approach can not only provide the colloidosome shells with controllable permeability but also avoid the excessive use of organic solvents with a simple and efficient encapsulation process. Some other researchers, such as Dinsmore et al.,[18] Routh and co-workers,[19,20] Sukhorukov et al.,[21] Nomura and Routh,[22] and Saunders and co-workers,[23] continued studying colloidosomes and extended to make some functional colloidosomes. For instance, Routh and co-workers[19,20] used P(MMA-BA) NPs as shell materials and environmentally friendly vegetable oil or sunflower oil as the oil phase to form stable colloidosomes with uniform shell porosities. Stark et al.[24] reported a simplified method wherein an impermeable

Received: October 7, 2023
Revised: December 7, 2023
Accepted: December 26, 2023
Published: January 11, 2024

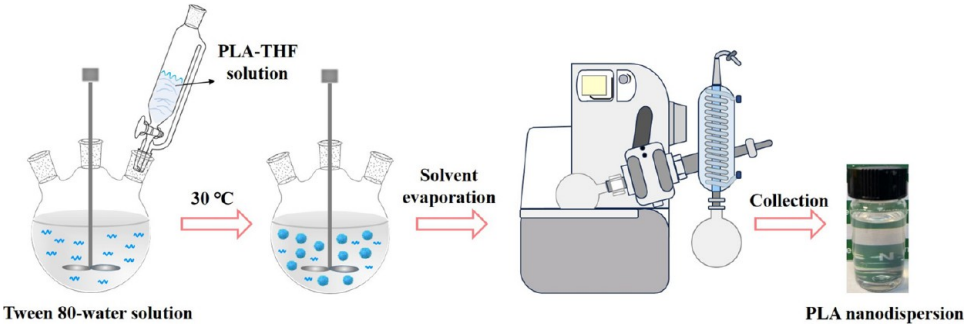

Figure 1. Preparation process of PLA nanodispersion.

metallic shell was deposited directly onto oil-in-water emulsion droplets. This process avoided the use of harmful solvents, and the metal shells provided microcapsules with an impermeable property. These above preparation methods used non-degradable materials as shells and have a relatively low encapsulation efficiency (EE). When using colloidosomes as drug carriers, especially for medicine and agriculture fields, both the shell properties and synthesis process are crucial to the EE and release performance. Therefore, it is urgent to develop a simple and mild preparation method for colloidosomes with degradable and nontoxic shells.

Polylactic acid (PLA) is a kind of widely used biodegradable polymer with low toxicity,[25] which can be completely degraded by microorganisms and has been approved by the Food and Drug Administration (FDA).[26] Based on its good biodegradability and high biocompatibility, PLA is widely applied in medical implantation, surgical sutures, and pesticide controlling release systems.[27−29] In order to obtain homogeneous and well-dispersed PLA NPs, an antisolvent precipitation method can be considered. During the precipitation process, the as-prepared particles were formed depending on the different supersaturation levels through the mixing of solvent and antisolvent.[30] When PLA NPs are used as shell materials, their dispersibility is crucial to the achievement of intact colloidosomes.

The spray drying method is frequently employed in industrial applications for the preparation of microcapsules due to its continuous production capability.[31] Microdroplets produced by spray drying serve as confined spaces, wherein rapid solvent evaporation leads to the formation of dried microcapsules.[32] As a result, this technique enables the fabrication of microcapsules with narrow size distributions and facilitates the in situ encapsulation of core materials within microcapsule shells. Traditional microcapsule shells made from materials like starch have found widespread use, but their shells may limit the potential for diverse design possibilities.[33,34] Liu et al. demonstrated a novel approach by successfully assembling latex particles at the water−air interface using a spray drying strategy, resulting in colloidosomes encapsulating small molecules.[35,36] The tunable shell permeability of these colloidosomes was achieved by adjusting the latex particle size and glass transition temperature. The design of colloidosomes through the selection and manipulation of nanoparticles holds promising avenues for extensive research exploration.

In this work, we introduce a novel method for the large-scale preparation of PLA colloidosomes with controllable permeability and high encapsulation efficiency. The shell materials PLA NPs were synthesized using an antisolvent precipitation method, and the possible formation mechanism was given through molecular dynamics (MD) simulation. By using the unmodified and Tween 80 modified PLA NPs, colloidosomes with controllable shell porosities can be easily constructed using spray drying technology. The optimum reaction conditions and formation mechanism of PLA colloidosomes were also revealed. Furthermore, AVM was used as a model for in situ encapsulation and controllable release. The UV-shielding properties of the colloidosomes were also tested.

2. EXPERIMENTAL SECTION

2.1. Materials and Equipment. Polylactic acid (PLA, M_w ∼ 80,000) was bought from Shanghai Maclin Biochemical Technology Co., Ltd. Polysorbate 80 (Tween 80, AR) was obtained from the Tianjin Damao Chemical Reagent Factory. Tetrahydrofuran (THF, AR) was purchased from Sinopharm Chemical Reagent Co. Ltd. Avermectin (AVM, 97%) was obtained from Shanghai Yuanye Biotechnology Co. Ltd. Acetone (AR) was purchased from Chengdu Colon Chemical Co. Ltd. Methanol (AR) was purchased from Guangdong Guanghua Sci-Tech Co., Ltd. Deionized water was filtered by a water purification system from Shanghai Hitech Instruments Co., Ltd. The spray dryer (L-317) was purchased from Beijing Laiheng Technology Co., Ltd. The rotary evaporators (Chem Tron STRIKE-380) and the ultrasonic homogenizer (SCIENTZ-IID) were purchased from Ningbo Xinzhi Biotechnology Co., Ltd.

2.2. Synthesis of PLA Nanodispersions as Shell Materials. Figure 1 shows the preparation process of the PLA nanodispersion. THF and deionized water were used as solvent and antisolvent, respectively. Original PLA polymers were dissolved in THF at 60 °C in a sealed container to form a PLA-THF solution with a concentration of 2.3 mg/mL. 28.6 wt % Tween 80 aqueous solution was poured into a three-necked flask and stirred, and then, the PLA-THF solution was dripped into the above solution. After stirring for a while, the prepared PLA suspension was evaporated at 30 °C in a rotary vacuum evaporator to remove the THF, and the aqueous PLA nanodispersion was obtained. The as-prepared PLA nanodispersion was adjusted to a certain concentration as shell materials for further colloidosome preparation.

2.3. Preparation of PLA Colloidosomes. The preparation process of colloidosomes by a spray drying method is displayed in Figure 2. Both distilled water and acetone were used to adjust the PLA nanodispersion with 0.15 mg/mL PLA concentration and 33.3 vol % acetone. The PLA nanodispersion was injected by a peristaltic pump into the spray dryer and atomized at a certain feed rate, compressed air flow rate, and inlet and outlet temperature. In a typical preparation process, the PLA nanodispersion was atomized into liquid

https://doi.org/10.1021/acsomega.3c07802
ACS Omega 2024, 9, 3781−3792

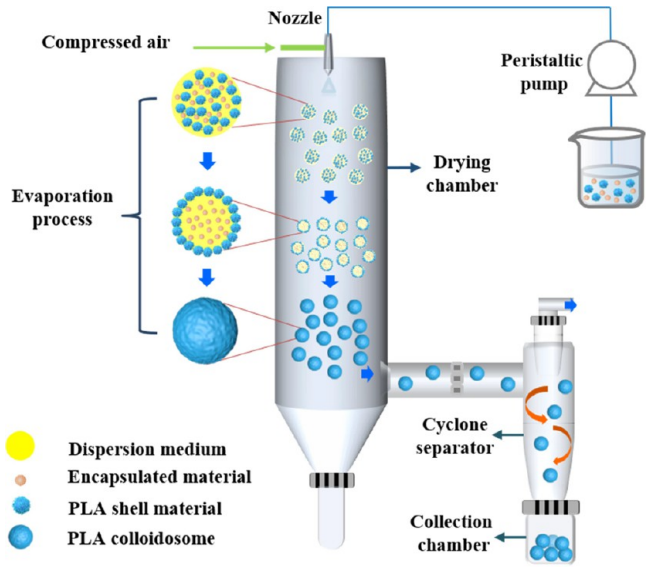

Figure 2. Preparation process of colloidosomes using a spray drying method.

microdroplets in a nozzle at a feed rate of 5.75 mL/min, a compressed air flow rate of 8 L/min, an inlet temperature of 140 °C, and an outlet temperature of 80 °C. The dispersion medium (water and acetone) in each microdroplet was quickly evaporated in a drying chamber. The PLA colloidosome products were then separated from a gas stream by a cyclone separator and collected by a collection chamber.

2.4. Encapsulation and Release of AVM. The procedure for preparing AVM-loaded PLA colloidosomes is basically the same as that of the above preparation process. The only difference is that the mixture solution contains 20 wt % of AVM to form the AVM-loaded colloidosomes and is stored at room temperature for a few days to ensure the shell pores are completely blocked. In a typical AVM release experiment, 20 mg of AVM-loaded colloidosomes was put into 100 mL of methanol−water (1:1) solvent in a sealed container wrapped with tin foil, and the container with AVM-loaded colloidosome suspensions was stirred at 300 rpm in the dark at room temperature. Then 3 mL of the liquid sample was taken at various times and was characterized by an ultraviolet−visible spectrophotometer in a quartz cuvette. The absorbance was recorded at 245 nm of absorbance value using methanol/water (1:1) as the reference.

$$\text{AVM release (\%)} = \frac{\text{amount of released AVM}}{\text{amount of total AVM}} \times 100$$

2.5. UV-Shielding Experiment. To test the UV-shielding properties of PLA colloidosomes, 20 mg of AVM-loaded colloidosomes were kept in the culture dish and sealed by plastic wrap, and then exposed to ultraviolet light irradiation (254 nm) at a distance of 25 cm from the light source. Twenty milligrams of AVM-loaded colloidosomes after ultrasound treatment were used as a control sample. For ultrasound treatment, the AVM-loaded colloidosomes were dispersed in 50 mL of methanol solution, and then an ultrasound probe (ultrasonic homogenizer) was introduced to break the colloidosomes operating at 600 kW for 2 min; 3.6 mg of pure AVM was basically consistent with the release amount of AVM obtained after ultrasonic treatment of colloidosomes. Three milliliters of sample solution was taken out using a syringe filter and was tested by an ultraviolet−visible spectrophotometer every 12 h. The degradation amounts of the AVM were measured by absorbance at 245 nm.

2.6. Molecular Dynamics Simulation. *2.6.1. Modeling and Molecular Structures.* The molecular structures were built with Materials Studio software, which is displayed in Figure 3. It had been reported that the few repeating units may represent the conformation of real polymer chains. In view of the flexible group of polylactic acid molecules, the low degree of polymerization may make it difficult to show their properties; therefore, we chose a molecular model with a degree of polymerization of 100.[37] In addition, shorter polymerization chains were preferred in order to provide a higher success rate of compaction.[38] By employing shorter chains of polymeric membrane instead of longer ones, the possibility of chain entanglement that may increase the intermolecular resistance during molecular dynamics simulation was prevented.[39]

The details of the simulation systems are listed in Table 1. The number of molecules was basically consistent with the data involved in the experimental process, and all components were blended randomly at the initial configuration by using Packmol software.

2.6.2. Simulation Details. The molecular dynamics simulation was operated by the GROMACS 2020.4 software package[40] with an OPLS-AA all-atom force field. The energy of

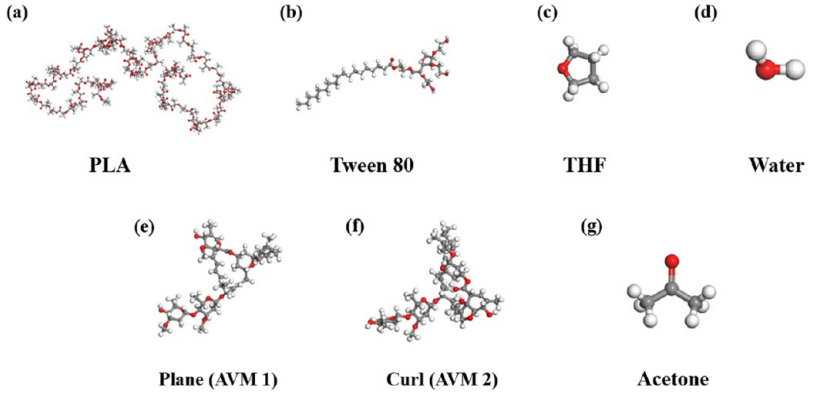

Figure 3. Molecular structures of all-atoms: (a) PLA, (b) Tween 80, (c) THF, (d) water, (e, f) different structural formulas of AVM, and (g) acetone. The carbon atoms, oxygen atoms, and hydrogen atoms are, respectively, in gray, red, and white colors.

https://doi.org/10.1021/acsomega.3c07802
ACS Omega 2024, 9, 3781−3792

Table 1. Details of Simulation Systems: System Type and Number of Each Component

		amount			
system name	box size (nm^3)	PLA	Tween 80	THF	water
particle formation	30 × 30 × 30	35	168	1320	90,300

the whole system was minimized by the steepest descent minimization. The step number and step size were 10,000 and 0.01 ps, respectively. After the energy of the whole system was minimized, NPT simulations were performed in 2 ns in order to briefly observe the nucleation process. In all simulations, all three directions applied periodic boundary conditions. The pressure was sustained at 1 bar with the Berendsen barostat, and the coupling constant was 20 ps. The temperature was maintained at 300 K with a V-rescale thermostat and a coupling constant of 0.1 ps. The ambient temperature and pressure for the molecular simulation were consistent with the experimental situation. Hydrogen bonds were constrained by the LINCS algorithm. The particle-mesh Ewald summation was used for van der Waals interactions with a cutoff of 1.2 nm[41] during all simulations. Then, a 40 ns NPT simulation was carried out to ensure the stability of the nuclear structure and observe the changes of gyrate radius. In the simulation, the data were analyzed to ensure that the entire system had reached an equilibrium state. The simulated trajectory was analyzed by the GROMACS 2020.4 software package.

The nonequilibrium molecular dynamics method was used to investigate the mechanism of AVM bounding to the interior of PLA colloidosomes. A box with x/y = 9 nm and z = 40 nm was built, which eliminated the periodic boundary conditions in the z direction and used virtual walls at both ends of the z direction. The numbers of water and acetone molecules in the system were 1220 and 150, respectively. The small number of water molecules was assumed since the temperature of nucleation was estimated to be above 100 °C; at this time, the water molecules were in the form of gas, and the corresponding number of molecules would be fewer. In view of the many configurations of avermectin, two different structural configurations of the plane and curl were used in the simulation, named AVM1 and AVM2, respectively. At the beginning of the simulation, the thrust was applied to the AVM1 and AVM2, running a 50 ps NPT simulation with temperature controlled at 370 K and pressure controlled at 1 bar. A 60 ns NVT simulation was then used to observe the movement of the molecules. In particular, in order to maintain the temperature of the solvent at its boiling point, we separately controlled the temperature of the solvent in the system to avoid regional temperature differences due to the irregular movement of molecules. Based on cyclic temperature control compression and suitable simulation results, the maximum pore diameter of the membrane material was 25.1 Å, and the maximum cavity diameter was 31.0 Å, which was similar to the two pore sizes obtained by the experiment (25.2 and 31.8 Å).

2.7. Characterization. The size and morphology of colloidosomes were observed by a scanning electron microscope (SEM, FEI Quattro S, Czech) at an accelerating voltage of 10.0 or 5.0 kV. The size and morphology of shell particles were imaged by a transmission electron microscope (TEM, HT7700, Japan) at an accelerating voltage of 100.0 kV. The Nano Measurer software was used to measure particle size on SEM and TEM images. Fourier transform infrared spectroscopy (FTIR, Nicolet Instrument Co., USA) was used to confirm the chemical component of shell particles and colloidosomes in the frequency range of 4000−400 cm^{-1}. The glass transition temperature (T_g) was tested by differential scanning calorimetry (DSC, DSC200PC, Germany). The aperture size distribution was measured based on N_2 adsorption−desorption by Micromeritics APSP 2460. The amount of AVM in the methanol−water solvent was measured by an ultraviolet−visible spectrophotometer (UV670, Meipuda, China) at a wavelength of 245 nm. The remains of AVM during the photodegradation process were estimated by an ultraviolet analyzer (ZF-8N, Jiapeng, China) at a wavelength of 254 nm with a power of 6 W.

3. RESULTS AND DISCUSSION

3.1. Preparation of Shell Particles. For an antisolvent precipitation process, the surfactants can be used to control the growth and dispersibility of particles by electrostatic or steric stabilization. In order to get well-dispersed PLA NPs, we choose to use Tween 80 as the surfactant, which is a kind of biodegradable nonionic surfactant. Figure 4 presents the possible mechanism of the formation of PLA nanodispersions. In a typical preparation process, THF was used as solvent dissolving PLA molecules, and water was used as an antisolvent containing Tween 80 molecules. The PLA NPs can be synthesized through nucleation, growth, and solvent evaporation steps. The effects of antisolvent/solvent ratio, temperature, and dosage of surfactant Tween 80 were explored.

3.1.1. Effect of Antisolvent/Solvent Ratio. The antisolvent/solvent (AS/S) ratio is an important factor for the precipitation

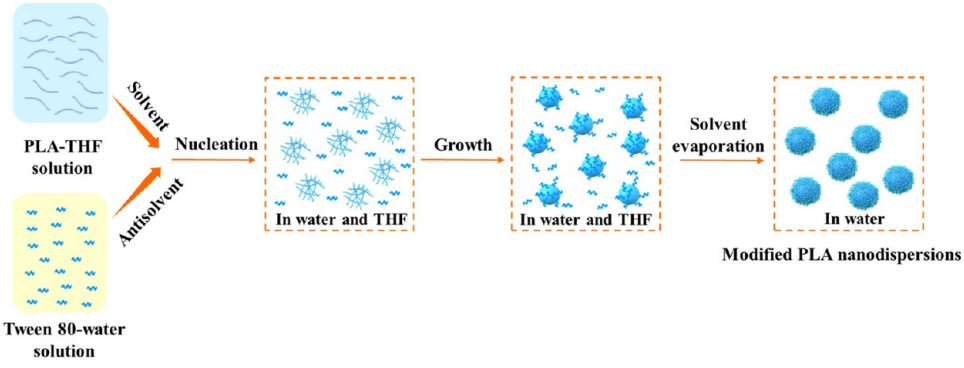

Figure 4. Possible formation mechanism of PLA nanodispersions.

https://doi.org/10.1021/acsomega.3c07802
ACS Omega 2024, 9, 3781−3792

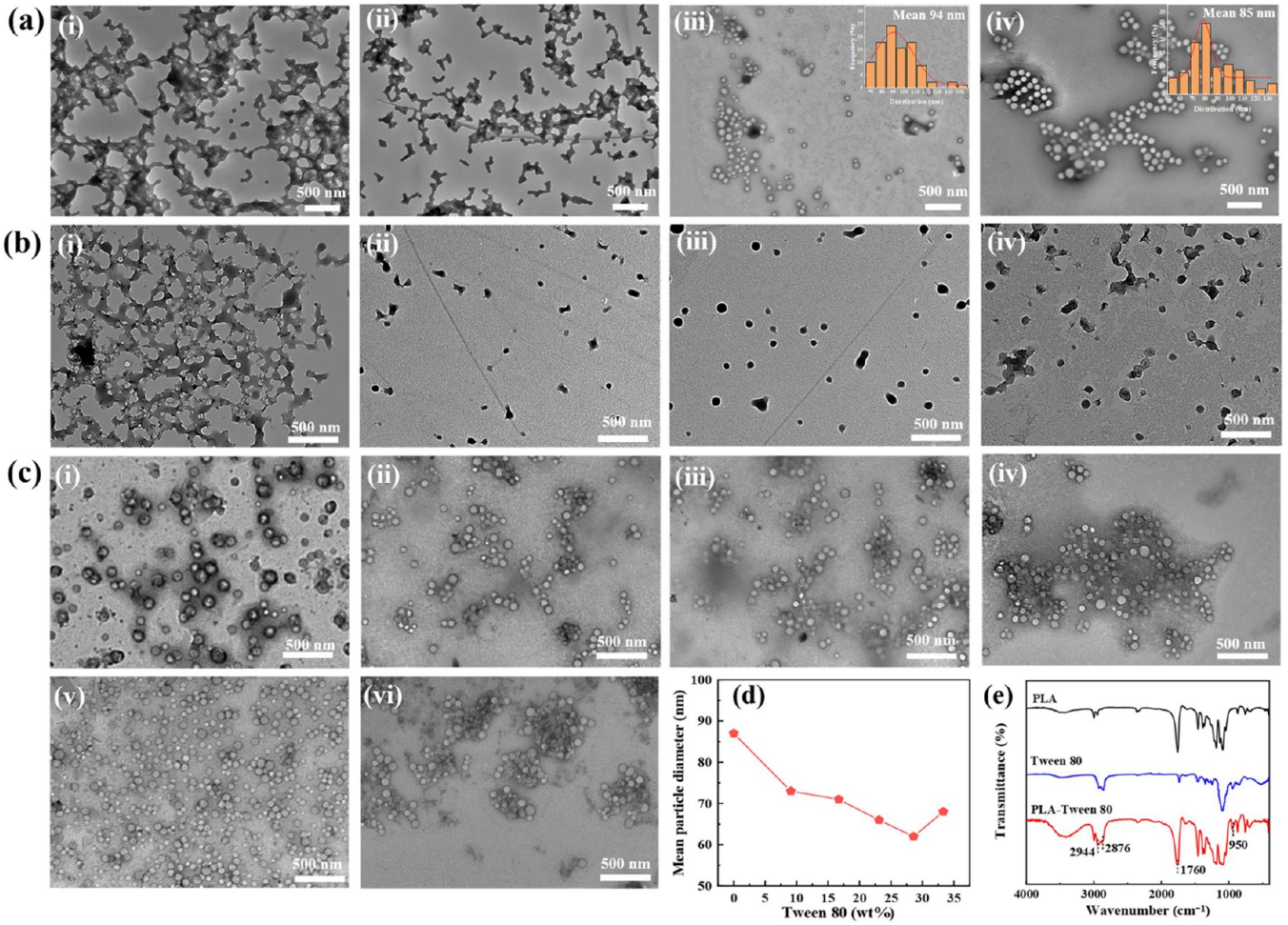

Figure 5. TEM images of PLA NPs prepared with different (a) AS/S ratios: (i) AS/S = 1, (ii) AS/S = 5, (iii) AS/S = 10, and (iv) AS/S = 15. (b) Temperatures: (i) 10 °C, (ii) 20 °C, (iii) 30 °C, and (iv) 40 °C. (c) Dosage of Tween 80: (i) 0 wt %, (ii) 9.1 wt %, (iii) 16.7 wt %, (iv) 23.1 wt %, (v) 28.6 wt %, and (vi) 33.3 wt %. (d) Mean diameter of PLA NPs using different dosages of Tween 80. (e) FTIR spectra of pure PLA, Tween 80, and Tween 80 modified PLA NPs.

process, as the driving force for precipitation is the supersaturation of the mixing solution, which is achieved through the rapid mixing of antisolvent (water) and solvent (THF). The TEM images of PLA NPs prepared at different AS/S ratios are depicted in Figure 5a. When the AS/S ratio is 1 or 5, the PLA NPs tend to heavily aggregate, which is unfavorable for them to be used as shell materials. As the AS/S ratio increases to 10 or 15, the aggregation of PLA NPs diminishes and the dispersibility of the PLA NPs remains favorable. In addition, as the AS/S ratio increases from 10 to 15, the size of PLA NPs slightly decreases from 94 to 85 nm. When increasing the AS/S ratio, the supersaturation of the mixing solution is increased due to the decrease in saturation concentration, leading to a faster nucleation rate.[42] Therefore, the different AS/S ratios have an obvious impact on particle dispersibility. When changing the AS/S ratios, as the PLA concentration in the original THF solution is fixed, the final PLA concentrations after mixing solvent and antisolvent are different, which also has an effect on particle size (Figure S2).

3.1.2. Effect of Temperature. Figure 5b shows the TEM images of PLA NPs prepared at different temperatures. As can be seen, the PLA NPs display an aggregated state when prepared at 10 °C. At a low temperature, the Brownian motion of the particles is weak, which may result in the PLA NPs agglomerating together during the particle growth process. As the temperature increases to 20−40 °C, the dispersibility of PLA NPs is highly improved since the particle Brownian motion becomes intensified, which can attenuate the agglomeration between particles. At 20 and 30 °C, the PLA NPs exhibit better dispersibility and smaller size. As the temperature further increases to 40 °C, the collision between PLA NPs intensifies, leading to particle slight adhesion.[43]

3.1.3. Effect of Dosage of Tween 80. Figure 5c,d presents the TEM images and mean diameter of PLA NPs using different dosages of Tween 80, which is m(Tween 80)/(m(Tween 80) + m(PLA)). When the Tween 80 dosage rises from 0 to 28.6 wt %, the mean size of PLA NPs reduces from 87 to 62 nm and the particle morphologies are getting closer to regular spherical. Further increasing the dosage of Tween 80 causes an obvious increase of particle size to 68 nm and a partial aggregation of PLA NPs. This result is because Tween 80 molecules can adsorb onto the hydrophobic surface of PLA NPs, forming a spatial stabilizing layer and inhibiting further growth. However, with further usage of Tween 80, the excess of Tween 80 causes intermolecular adhesion and intertwining, which may diminish the dispersibility of PLA NPs.

The PLA NPs prepared with an AS/S ratio of 15, 28.6 wt % dosage of Tween 80, and 30 °C were used as shell materials for

https://doi.org/10.1021/acsomega.3c07802
ACS Omega 2024, 9, 3781−3792

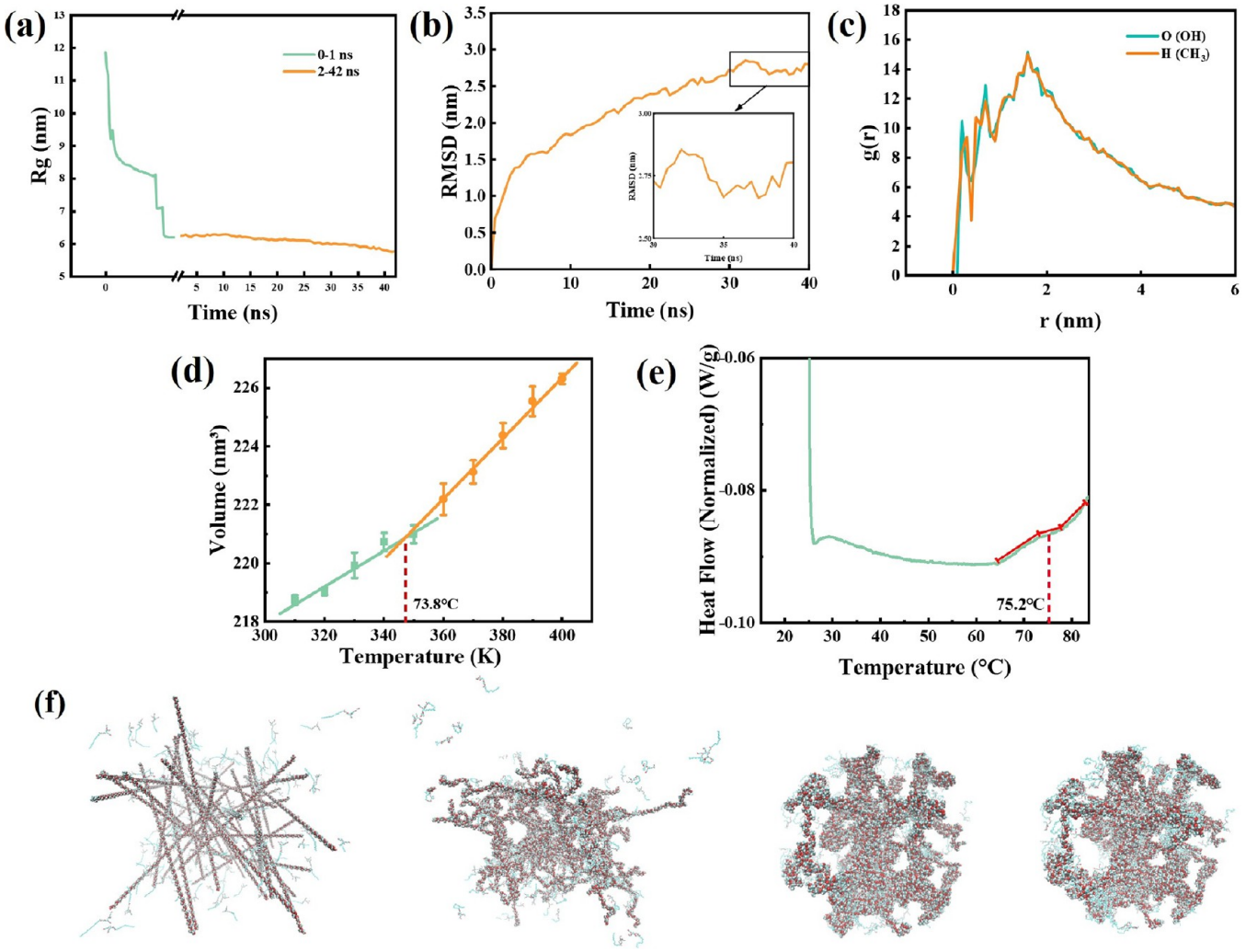

Figure 6. (a) *Rg* curves of PLA molecules in first 1 ns, (b) RMSD curves of the PLA molecules, (c) RDF about the centroid of atoms, (d, e) T_g curves of modified PLA particles, respectively, in simulation and experiment, and (f) representative snapshots of the formation of modified PLA particles.

further preparation of colloidosomes. Figure 5e presents the FTIR spectra of pure PLA, Tween 80, and Tween 80 modified PLA NPs. As can be seen, for Tween 80 modified PLA NPs, the characteristic absorption peaks at 2944 and 2876 cm^{-1} are assigned to asymmetric and symmetric stretching of the methylene groups ($-CH_2-$). The peaks at 1760 and 950 cm^{-1} are assigned to the C═O (ester group) stretching vibrations and the bending vibrations of C−H. This indicates that the PLA NPs are successfully modified by using Tween 80 as a surfactant.

3.2. MD Simulation. *3.2.1. Forming Analysis of Particles.* In the solution, due to the influence of thermal motion, large molecules like polymer molecules are constantly twisted, bent, and vibrated.[44] The radius of gyration (ROG) is a physical quantity that describes the result of this motion. The ROG decreases with the increase in simulation time. As shown in Figure 6a, the PLA molecules nucleate and grow within the first 1 ns, and then, the ROG value slowly decreases and eventually fluctuates in a small range within 40 ns. This shows that the PLA molecules have a dense structure, and the particles take shape. The root-mean-square deviation (RMSD) value also indicates that the molecules tend to be stable. The RMSD describes the index of difference between the molecular structures and the initial structure at each moment of the simulation.[45] The RMSD value of the PLA molecules reaches a steady value after 30 ns and varies in a small range until 40 ns in Figure 6b, indicating that PLA molecules reach a relatively stable structure.

3.2.2. Stability Analysis of the System. The radial distribution function (RDF) about the centroid of atoms (Figure 6c) exhibits the same peak position at the same location, which illustrates that the hydrogen atoms on the alkyl group of Tween 80 have higher adsorption with the double-bonded oxygen atoms on the polylactic acid chains. Similarly, the oxygen atoms on the hydroxyl group are also highly adsorbed. The location of the highest peaks makes the intensity of the interaction similar. This causes the Tween 80 molecules to attach to the surface of the polylactic acid molecules in a similar tiled form with strong adsorption at both ends. Stable values tended to 0, demonstrating that the radial distance reaches beyond the sample volume.[46]

3.2.3. Combination of Theory and Experiment. The theoretical and experimental values of the glass transition temperature of modified PLA particles are, respectively, shown in Figure 6d,e. The theoretical values are basically consistent

https://doi.org/10.1021/acsomega.3c07802
ACS Omega 2024, 9, 3781−3792

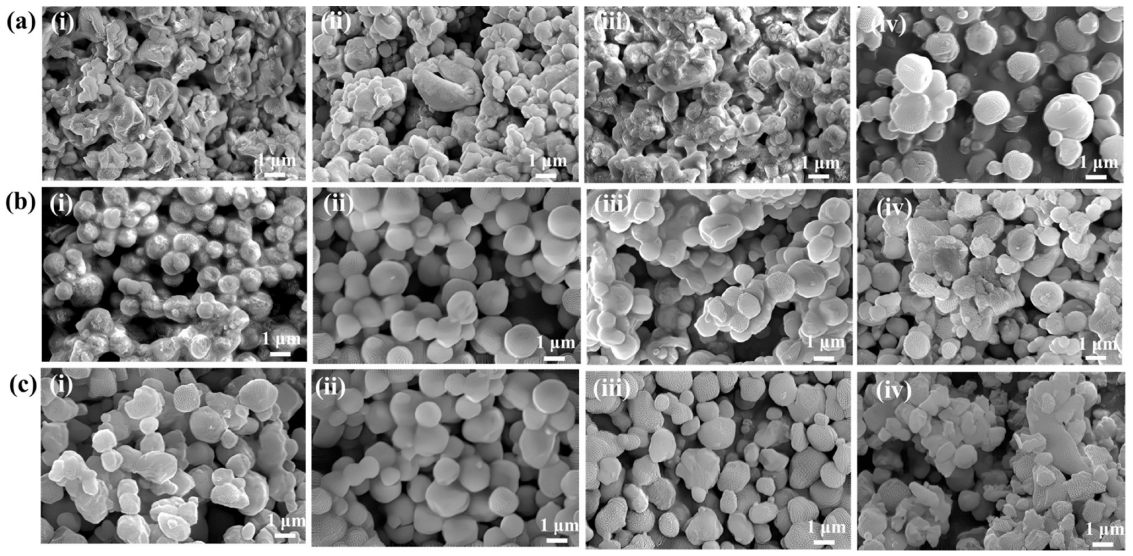

Figure 7. SEM images of colloidosomes prepared with different (a) inlet temperatures: (i) 80 °C, (ii) 100 °C, (iii) 120 °C, and (iv) 140 °C. (b) Feed rate: (i) 5.0 mL/min, (ii) 5.75 mL/min, (iii) 6.5 mL/min, and (iv) 7.25 mL/min. (c) Flow rates of compressed air: (i) 5 L/min, (ii) 8 L/min, (iii) 10 L/min, and (iv) 13 L/min.

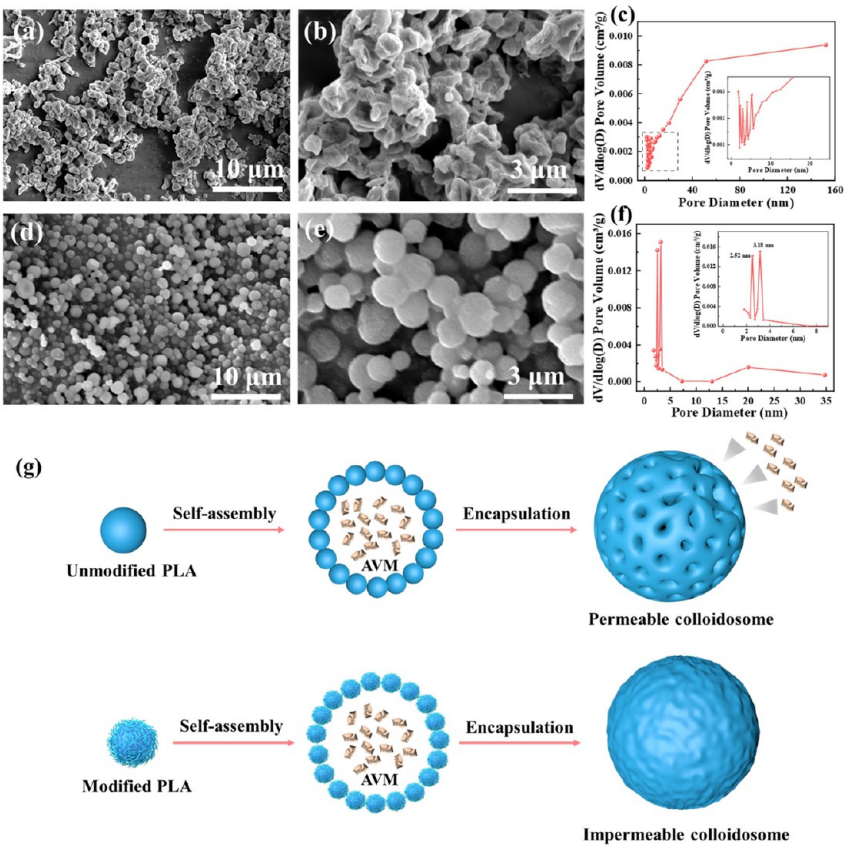

Figure 8. SEM images of colloidosomes using (a, b) unmodified and (d, e) modified PLA NPs as shell materials, (c, f) pore diameter distribution of the colloidosomes, and (g) synthetic mechanism of permeable and impermeable colloidosomes.

with the experimental values, indicating the particles were successfully formed.

3.2.4. Dynamic Simulation. The nucleation and growth process of particles is shown in Figure 6f. The PLA molecules first nucleate; then, some Tween 80 molecules are adsorbed on its surface during the growth process, and finally, Tween 80 molecules are coated on the surface of the PLA particles to form a stable system.

3.3. Preparation of Colloidosomes. The formation mechanism of colloidosomes is shown in Figure 2. As can be seen, the dispersion of PLA NPs is atomized into micro-droplets by compressed air at the nozzle. Due to their hydrophobic nature, the PLA NPs will migrate to the surface of

https://doi.org/10.1021/acsomega.3c07802
ACS Omega 2024, 9, 3781−3792

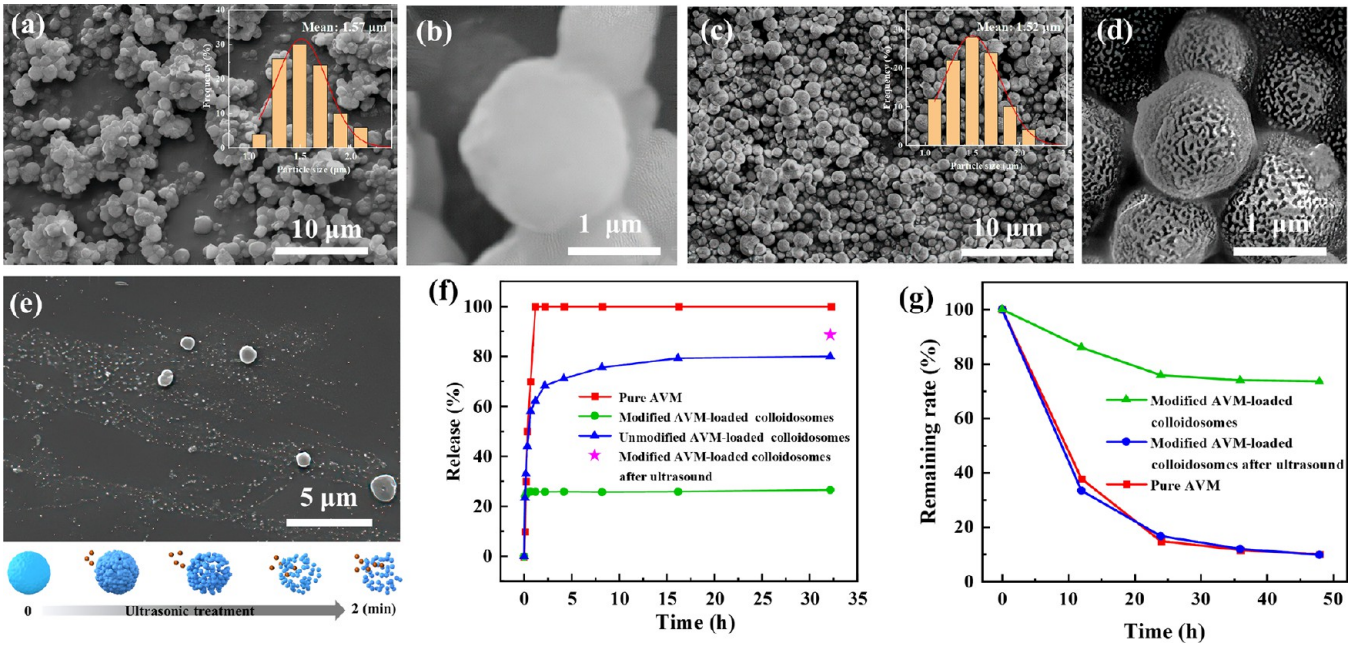

Figure 9. SEM images of (a, b) modified AVM-loaded colloidosomes, (c, d) unmodified AVM-loaded colloidosomes, (e) SEM image and diagram of modified AVM-loaded colloidosomes after ultrasound treatment, (f) AVM release, and (g) remaining rate curves of pure AVM and different colloidosome samples.

microdroplets, concurrent with solvent evaporation. As the particles come into contact, an outer shell forms, and the dispersion molecules (water and acetone) continue to evaporate from the core. Finally, the drying process is finished, and the colloidosomes can be formed; as-prepared colloidosomes are gathered in the collection chamber. The morphologies and sizes of PLA colloidosomes can be influenced by the spray drying parameters, for instance, inlet temperatures, feed rates, and compressed air flow rates. The TEM and size distribution images of PLA NPs dispersed in water and water−acetone solution are shown in Figure S2.

3.3.1. Effect of Inlet Temperature. Figure 7a presents the SEM images of colloidosomes prepared at different inlet temperatures. When increasing the inlet temperature, the colloidosomes have a more spherical shape and better dispersity. At the temperatures of 80, 100, and 120 °C, the colloidosomes are shrunk, broken, and unshaped. One potential factor is that during the evaporation of liquids inside the shells, the heat transfer rate of the internal hot air is slower than that of the external air, leading to a pressure difference between the interior and exterior. At a temperature of 140 °C, the partial evaporation of Tween 80 helps equalize the pressure inside and outside the colloidosomes, resulting in the formation of spherical colloidosomes with reduced instances of rupture.

3.3.2. Effect of Feed Rate. The influence of the feed rate on the colloidosome morphology is illustrated in Figure 7b. At a low feed rate (5.0 mL/min), the colloidosomes exhibit spherical shapes with some degree of agglomeration between them. A lower feed rate implies reduced liquid drying, causing the products to remain exposed to hot air for a relatively extended period, which may lead to adhesion between colloidosomes. As the feed rate increases to 5.75 mL/min, the colloidosomes assume a more well-defined spherical form. However, with further escalation of the feed rate (6.5−7.25 mL/min), the uneven droplet sizes result in colloidosomes losing their consistency and size uniformity, and the mutual adhesion of colloidosomes is potentially attributed to the insufficient time for some Tween 80 evaporating.

3.3.3. Effect of Compressed Air Flow Rate. Figure 7c depicts the distinct morphologies of colloidosomes prepared under various flow rates of compressed air. Under a low flow rate of 5 L/min, the PLA colloidosomes exhibit poor sphericity. As the flow rate increases to 8 L/min, the colloidosomes display uniformly spherical structures. When the compressed air flow rate further escalates to 10 and 13 L/min, the microdroplets of varying sizes result in a wide size distribution of colloidosomes and lead to adhesion between colloidosomes. Moreover, the extended heating time also leads to contraction and rupture of the polymer shells.

For the colloidosome preparation process, Tween 80 as the surfactant may remain within or between shell particles, contributing to the structural stability of the colloidosomes, thereby preventing shell collapse. The usage of Tween 80 also leads to an increased level of colloidosome sphericity, which can be observed by comparing SEM images of colloidosomes using modified and unmodified PLA NPs in Figure 8a,b,d,e. By using the modified and unmodified PLA NPs as shell materials, colloidosomes with controllable shell porosities can be easily constructed using spray drying technology. The pore diameter distribution of colloidosomes prepared with unmodified and modified PLA NPs as shell materials can be obtained using the BJH model of the desorption branch of the N_2 isotherms with an automatic surface and aperture analyzer. The pore size distribution of colloidosomes using unmodified PLA NPs is relatively wide and uneven (Figure 8c). In contrast, the usage of Tween 80 results in a reduction in the pore size diameter to around 2.52 and 3.18 nm (Figure 8f). The synthetic mechanism of permeable and impermeable colloidosomes can be seen in Figure 8g.

3.4. AVM Encapsulation. AVM was used as a model for in situ encapsulation and controllable release. The SEM images

https://doi.org/10.1021/acsomega.3c07802
ACS Omega 2024, 9, 3781−3792

Table 2. Published Studies on Spray Drying Drug Delivery Applications[a]

type of drugs	shell materials	solvent	encapsulation efficiency (%)	references
cyclosporin	PLGA	DCM, ethanol	37.8−41.4	47
dexamethasone	PLGA	DCM, ethanol	62.4−80.7	47
acyclovir	semisynthetic biopolymer complex	water, DCM	85.0	48
walnut oil	skim milk powder, Tween 80	water	91.0	49
walnut oil	soybean protein, maltodextrin	water	72.2	50
avermectin	PLA, Tween 80	water, acetone	89.7	this work

[a]The encapsulation efficiency (%) = amount of drug in microcapsules/initial drug amount.

and corresponding size distributions of AVM-loaded colloidosomes, using both unmodified and Tween 80 modified PLA NPs as shell materials, are shown in Figure 9a−d. After encapsulation, both the modified and unmodified colloidosomes exhibit a uniform spherical morphology with an average diameter of 1.57 and 1.52 μm, respectively. However, there is adhesion among the modified AVM-loaded colloidosomes, whereas the unmodified AVM-colloidosomes exhibit a more obvious and dispersed spherical structure with larger pores. The FTIR spectra of pure AVM, PLA colloidosomes, and AVM-loaded PLA colloidosomes are depicted in Figure S1, showing the successful encapsulation of AVM in the colloidosomes. In addition, the as-prepared colloidosomes are ultrasound-responsive. As shown in Figure 9e, after 2 min ultrasound treatment, there exist a few intact colloidosomes and a large amount of broken pieces of shells.

Figure 9f shows the AVM release curves of pure AVM, unmodified AVM-loaded colloidosomes, modified AVM-loaded colloidosomes, and modified AVM-loaded colloidosomes after ultrasound treatment. As can be seen, the pure AVM sample dissolves rapidly within 2 h. In contrast, the unmodified AVM-loaded colloidosome sample exhibits sustained release, showing a release percentage of approximately 80% within 32 h. While the release rate of modified AVM-loaded colloidosomes shows 27% only within 40 min. This quick release may be caused by the physical adsorption of AVM on the colloidosome surface. Then, the colloidosomes are nearly impermeable for even a relatively long time, which may be caused by the ultrasmall shell porosity. As the modified colloidosomes are ultrasound-responsive, the encapsulated AVM can be released from the impermeable shells by ultrasound treatment, showing a release percentage of 89.7%. This result also indicates the crucial role of Tween 80 in the controllable permeability of the colloidosomes.

Figure 9g shows the photodegradation curves of pure AVM, modified AVM-loaded colloidosomes, and modified AVM-loaded colloidosomes after ultrasound treatment. The two colloidosome samples encapsulate the same amount of AVM as pure AVM sample. After 12 h of UV light exposure, the pure AVM sample reveals a degradation rate of 63% and a degradation rate of 91% after 48 h. The modified AVM-loaded colloidosome sample after ultrasound treatment illustrates a similar trend to the pure AVM sample. In contrast, the modified AVM-loaded colloidosome sample shows a degradation rate of only 27% after 48 h. These results verify that the intact PLA colloidosomes reveal excellent UV-shielding properties, which can protect AVM from photodegradation. In addition, our colloidosomes exhibit higher encapsulation efficiency, compared with some published studies on spray drying drug delivery applications (Table 2).

3.5. Impermeability Properties of Colloidosomes. The molecular motion trajectory is shown in Figure 10. As the simulation progressed, the solvent molecules passed through the colloidosome shell material and reached equilibrium at both ends of the shell. However, the AVM molecules were blocked by the shell, and the interaction between the molecules caused them to be adsorbed on the inner wall of the shell. The number density diagram in the Z direction is shown in Figure 11a. At the surface of the shell (around 22.8 nm), the values of AVM1 and AVM2 reach their highest peaks and then decrease to 0. The water molecules maintain similar values on the shell surface and always maintain a certain value outside the shell material system.

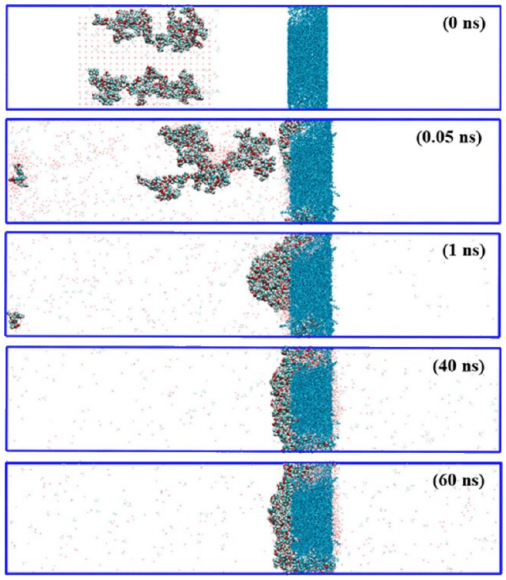

Figure 10. Molecular motion trajectory.

As shown in Figure 11b, the red and blue lines are the dynamic diameter ranges of AVM1 and AVM2, respectively. The green dots are the diameter of the modified PLA particle pore. The pore channel was measured at 0, 20, 40, and 60 ns, respectively. As the kinetic process of the drug molecules progressed, AVM1 and AVM2 were accumulated around the pore, causing the pore to decrease from 25.1 nm to an average of 9.5 nm, which was less than the minimum kinetic diameter of AVM. Even if the initial pore is large enough (exceeding the diameter of motion of the AVM), the AVM cannot pass through the membrane in subsequent simulations.

The two-dimensional map of the axial radial density is shown in Figure 11c. The figure on the left shows the number density distribution of AVM1 and AVM2, and the figure on the right shows the number density distribution of the film material. First, due to the periodic boundary conditions in the x/y direction, the upper and lower two-lobed blank area in the right figure is a complete hollow. The white part is the area with a low number density, and the darker color is the area

https://doi.org/10.1021/acsomega.3c07802
ACS Omega 2024, 9, 3781−3792

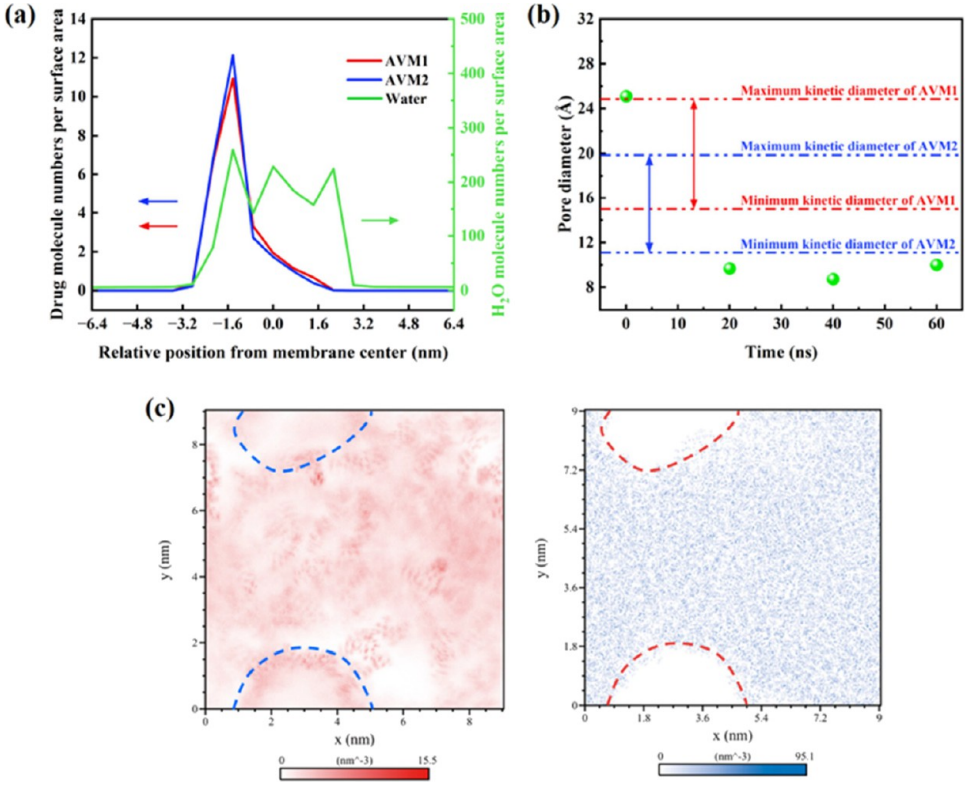

Figure 11. (a) Number density of molecules per surface area, (b) kinetic diameter of AVM and the pore diameter of modified PLA particles, and (c) number density distribution of AVM1 and AVM2.

with a higher number density. The red and blue dashed lines represent the same area. It can be found that in the blue dashed line at the bottom, the number density of AVM1 and AVM2 is high, indicating that pesticide molecules are blocking the pore. This also proves that the shell material can capture AVM molecules through molecular interaction and block the pore.

4. CONCLUSIONS

In this study, we report a concise and effective route for the large-scale preparation of biodegradable PLA colloidosomes. The PLA shell materials can be synthesized by using an antisolvent precipitation method. The factors of antisolvent/solvent ratio, PLA concentration, temperature, and dosage of surfactant Tween 80 were explored in detail, and the possible formation mechanism was given through the MD simulation. Tween 80 adsorbs on the surface of PLA particles to form a stable spatial barrier layer. Comparing the theoretical and experimental glass transition temperatures of PLA particles, the theoretical values are basically consistent with the experimental results. Furthermore, colloidosomes with controllable permeability can be easily constructed using the modified and unmodified PLA NPs by spray drying technology. The influences of inlet temperature, feed rate, and flow rates of compressed air on the morphologies of colloidosomes were also studied. The PLA colloidosomes can successfully encapsulate AVM with a high encapsulation efficiency of 89.7%, and the release durations of colloidosomes prepared with different PLA NPs range from 32 h to nearly impermeable, which can be further verified by the MD simulation. AVM molecules aggregate around the shell pores and cannot pass through the shell pores during the evaporation of water molecules. More importantly, the PLA colloidosomes also reveal excellent UV-shielding properties, which can protect AVM from photodegradation. Therefore, this work presents a promising way to prepare a controllable release of colloidosomes for pesticide encapsulation.

■ ASSOCIATED CONTENT

Supporting Information

The Supporting Information is available free of charge at https://pubs.acs.org/doi/10.1021/acsomega.3c07802.

FTIR spectra of pure AVM, PLA colloidosomes, and AVM-loaded PLA colloidosomes; TEM images of PLA NPs prepared with different PLA concentrations; and TEM and size distribution images of unmodified and modified PLA NPs in water and water−acetone solution (PDF)

■ AUTHOR INFORMATION

Corresponding Author

Qian Sun − *Guangxi Key Laboratory of Petrochemical Resource Processing and Process Intensification Technology and School of Chemistry and Chemical Engineering and State Key Laboratory of Featured Metal Materials and Life-Cycle Safety for Composite Structures, Guangxi University, Nanning 530004, China;* orcid.org/0000-0002-7492-0024; Email: sunqian@gxu.edu.cn

Authors

Zulipiker Payizila − *Guangxi Key Laboratory of Petrochemical Resource Processing and Process Intensification Technology and School of Chemistry and Chemical Engineering, Guangxi University, Nanning 530004, China*

https://doi.org/10.1021/acsomega.3c07802
ACS Omega 2024, 9, 3781−3792

Fuquan Teng − *Guangxi Key Laboratory of Petrochemical Resource Processing and Process Intensification Technology and School of Chemistry and Chemical Engineering, Guangxi University, Nanning 530004, China*

Xudong Huang − *Guangxi Key Laboratory of Petrochemical Resource Processing and Process Intensification Technology and School of Chemistry and Chemical Engineering, Guangxi University, Nanning 530004, China*

Wenbiao Liu − *Guangxi Key Laboratory of Petrochemical Resource Processing and Process Intensification Technology and School of Chemistry and Chemical Engineering, Guangxi University, Nanning 530004, China*

Tengfei Wu − *Guangxi Key Laboratory of Petrochemical Resource Processing and Process Intensification Technology and School of Chemistry and Chemical Engineering, Guangxi University, Nanning 530004, China*

Shuangliang Zhao − *Guangxi Key Laboratory of Petrochemical Resource Processing and Process Intensification Technology and School of Chemistry and Chemical Engineering and State Key Laboratory of Featured Metal Materials and Life-Cycle Safety for Composite Structures, Guangxi University, Nanning 530004, China;* orcid.org/0000-0002-9547-4860

Complete contact information is available at: https://pubs.acs.org/10.1021/acsomega.3c07802

Notes

The authors declare no competing financial interest.

■ ACKNOWLEDGMENTS

This work was financially supported by the National Natural Science Foundation of China (22168010), Guangxi Science and Technology Base and Special Funding for Talents (GuikeAD23026333), and the Dean Project of Guangxi Key Laboratory of Petrochemical Resource Processing and Process Intensification Technology (2021Z007).

■ REFERENCES

(1) Jia, J.; Liu, R. K.; Gu, Y. H.; Sun, Q.; Wang, J. X.; Chen, J. F. High-Gravity-Assisted Fabrication of Self-Assembled Colloidosomes. *Ind. Eng. Chem. Res.* **2022**, *61*, 6934−6944.

(2) Cheng, S. Y.; Yuen, M. C. W.; Kan, C. W.; Cheuk, K. K. L.; Chui, C. H.; Lam, K. H. Cosmetic Textiles with Biological Benefits: Gelatin Microcapsules Containing Vitamin C. *Int. J. Mol. Med.* **2009**, *24*, 411−419.

(3) Peña, B.; Panisello, C.; Aresté, G.; Garcia-Valls, R.; Gumí, T. Preparation and Characterization of Polysulfone Microcapsules for Perfume Release. *Chem. Eng. J.* **2012**, *179*, 394−403.

(4) Illésová, A.; Bučko, M.; Vikartovská, A.; Gemeiner, P. Encapsulation as a Useful Tool for a Biotechnological Production of Natural Aromas. *Curr. Opin. Biotechnol.* **2013**, *24*, 59−60.

(5) Yang, X. L.; Ju, X. J.; Mu, X. T.; Wang, W.; Xie, R.; Liu, Z.; Chu, L. Y. Core-Shell Chitosan Microcapsules for Programmed Sequential Drug Release. *ACS Appl. Mater. Interfaces* **2016**, *8*, 10524−10534.

(6) Varona, S.; Kareth, S.; Martín, Á.; Cocero, M. J. Formulation of Lavandin Essential Oil with Biopolymers by PGSS for Application as Biocide in Ecological Agriculture. *J. Supercriti. Fluid.* **2010**, *54*, 369−377.

(7) Zhao, M.; Chen, Z.; Hao, L.; Chen, H.; Zhou, X.; Zhou, H. CMC Based Microcapsules for Smart Delivery of Pesticides with Reduced Risks to the Environment. *Carbohyd. Polym.* **2023**, *300*, No. 120260.

(8) Sun, Q.; Gao, H.; Sukhorukov, G. B.; Routh, A. F. Silver-Coated Colloidosomes as Carriers for an Anticancer Drug. *ACS Appl. Mater. Interfaces* **2017**, *9*, 32599−32606.

(9) Wang, H. C.; Grolman, J. M.; Rizvi, A.; Hisao, G. S.; Rienstra, C. M.; Zimmerman, S. C. pH-Triggered Release from Polyamide Microcapsules Prepared by Interfacial Polymerization of a Simple Diester Monomer. *ACS Macro Lett.* **2017**, *6*, 321−325.

(10) Sun, S.; Gao, Y.; Han, N.; Zhang, X.; Li, W. Reversible Photochromic Energy Storage Polyurea Microcapsules via In-Situ Polymerization. *Energy* **2021**, *219*, No. 119630.

(11) Fan, J.; Zheng, Y.; Xie, Y.; Sun, Y.; Luan, Y.; Jiang, W.; Wang, C.; Liu, S.; Liu, X. Effect of Solvent Evaporation Technique on the Characteristics of Curing Agent Microcapsules and the Curing Process. *Compos. Sci. Technol.* **2017**, *138*, 80−90.

(12) Hitchcock, J. P.; Tasker, A. L.; Baxter, E. A.; Biggs, S.; Cayre, O. J. Long-Term Retention of Small, Volatile Molecular Species within Metallic Microcapsules. *ACS Appl. Mater. Interfaces* **2015**, *7*, 14808−14815.

(13) Zhang, K.; Wang, M.; Wu, M.; Wu, Q.; Liu, J.; Yang, J.; Zhang, J. One-Step Production of Amine-Functionalized Hollow Mesoporous Silica Microspheres via Phase Separation-Induced Cavity in Miniemulsion System for Opaque and Matting Coating. *Ind. Eng. Chem. Res.* **2020**, *59*, 723−731.

(14) Yin, D.; Bai, L.; Jia, Y.; Liu, J.; Zhang, Q. Microencapsulation through Thermally Sintering Pickering Emulsion-Based Colloidosomes. *Soft Matter* **2017**, *13*, 3720−3725.

(15) Douliez, J. P.; Martin, N.; Beneyton, T.; Eloi, J. C.; Chapel, J. P.; Navailles, L.; Baret, J. C.; Mann, S.; Béven, L. Preparation of Swellable Hydrogel-Containing Colloidosomes from Aqueous Two-Phase Pickering Emulsion Droplets. *Angew. Chem., Int. Ed.* **2018**, *57*, 7780−7784.

(16) Velev, O. D.; Furusawa, K.; Nagayama, K. Assembly of Latex Particles by Using Emulsion Droplets as Templates. 1. Microstructured Hollow Spheres. *Langmuir* **1996**, *12*, 2374−2384.

(17) Velev, O. D.; Nagayama, K. Assembly of Latex Particles by Using Emulsion Droplets. 3. Reverse (Water in Oil) System. *Langmuir* **1997**, *13*, 1856−1859.

(18) Dinsmore, A. D.; Hsu, M. F.; Nikolaides, M. G.; Marquez, M.; Bausch, A. R.; Weitz, D. A. Colloidosomes: Selectively Permeable Capsules Composed of Colloidal Particles. *Science* **2002**, *298*, 1006−1009.

(19) Keen, P. H. R.; Slater, N. K. H.; Routh, A. F. Encapsulation of Lactic Acid Bacteria in Colloidosomes. *Langmuir* **2012**, *28*, 16007−16014.

(20) Keen, P. H. R.; Slater, N. K. H.; Routh, A. F. Encapsulation of Yeast Cells in Colloidosomes. *Langmuir* **2012**, *28*, 1169−1174.

(21) Sukhorukov, G. B.; Rogach, A. L.; Zebli, B.; Liedl, T.; Skirtach, A. G.; Köhler, K.; Antipov, A. A.; Gaponik, N.; Susha, A. S.; Winterhalter, M.; Parak, W. J. Nanoengineered Polymer Capsules: Tools for Detection, Controlled Delivery, and Site-Specific Manipulation. *Small* **2005**, *1*, 194−200.

(22) Nomura, T.; Routh, A. F. A Novel Method of Fabrication of Latex-Stabilized Water-Core Colloidosomes at Room Temperature. *Langmuir* **2010**, *26*, 18676−18680.

(23) Wang, W.; Milani, A. H.; Cui, Z.; Zhu, M.; Saunders, B. R. Pickering Emulsions Stabilized by pH-Responsive Microgels and Their Scalable Transformation to Robust Submicrometer Colloidosomes with Selective Permeability. *Langmuir* **2017**, *33*, 8192−8200.

(24) Stark, K.; Hitchcock, J. P.; Fiaz, A.; White, A. L.; Baxter, E. A.; Biggs, S.; McLaughlan, J. R.; Freear, S.; Cayre, O. J. Encapsulation of Emulsion Droplets with Metal Shells for Subsequent Remote Triggered Release. *ACS Appl. Mater. Interfaces* **2019**, *11*, 12272−12282.

(25) Peres, C.; Matos, A. I.; Conniot, J.; Sainz, V.; Zupančič, E.; Silva, J. M.; Graça, L.; Sá Gaspar, R.; Préat, V.; Florindo, H. F. Poly (Lactic Acid)-Based Particulate Systems Are Promising Tools for Immune Modulation. *Acta Biomater.* **2017**, *48*, 41−57.

(26) Feng, C.; Yuan, X.; Chu, K.; Zhang, H.; Ji, W.; Rui, M. Preparation and Optimization of Poly (Lactic Acid) Nanoparticles Loaded with Fisetin to Improve Anti-Cancer Therapy. *Int. J. Biol. Macromol.* **2019**, *125*, 700−710.

(27) Fang, J.; Nakamura, H.; Maeda, H. The EPR Effect: Unique Features of Tumor Blood Vessels for Drug Delivery, Factors Involved, and Limitations and Augmentation of the Effect. *Adv. Drug Deliver. Rev.* **2011**, *63*, 136−151.
(28) Muro-Suñé, N.; Gani, R.; Bell, G.; Shirley, I. Model-Based Computer-Aided Design for Controlled Release of Pesticides. *Comput. Chem. Eng.* **2005**, *30*, 28−41.
(29) Liu, S.; Yu, J.; Li, H.; Wang, K.; Wu, G.; Wang, B.; Liu, M.; Zhang, Y.; Wang, P.; Zhang, J.; Wu, J.; Jing, Y.; Li, F.; Zhang, M. Controllable Drug Release Behavior of Polylactic Acid (PLA) Surgical Suture Coating with Ciprofloxacin (CPFX)-Polycaprolactone (PCL)/Polyglycolide (PGA). *Polymers* **2020**, *12*, 288.
(30) Shi, W.; Li, S.; Wang, X.; Li, S.; Zhang, X. Characterization and Properties of Hexaconazole-Loaded Nanoparticles Prepared by Anti-Solvent Method. *J. Drug Delivery Sci. Tec.* **2023**, *81*, No. 104288.
(31) Moser, P.; Nicoletti, V. R.; Drusch, S.; Brückner-Gühmann, M. Functional Properties of Chickpea Protein-Pectin Interfacial Complex in Buriti Oil Emulsions and Spray Dried Microcapsules. *Food Hydrocolloid.* **2020**, *107*, No. 105929.
(32) Zhang, L.; Wei, Y.; Liao, W.; Tong, Z.; Wang, Y.; Liu, J.; Gao, Y. Impact of Trehalose on Physicochemical Stability of β-Carotene High Loaded Microcapsules Fabricated by Wet-Milling Coupled with Spray Drying. *Food Hydrocolloid.* **2021**, *121*, No. 106977.
(33) Sun, Y.; Fan, S.; Liang, R.; Ni, X.; Du, Y.; Wang, J.; Yang, C. Design and Characterization of Starch/Solid Lipids Hybrid Microcapsules and Their Thermal Stability with Menthol. *Food Hydrocolloid.* **2021**, *116*, No. 106631.
(34) Dang, X.; Yang, M.; Shan, Z.; Mansouri, S.; May, B. K.; Chen, X.; Chen, H.; Woo, M. W. On Spray Drying of Oxidized Corn Starch Cross-Linked Gelatin Microcapsules for Drug Release. *Mater. Sci. Eng. C* **2017**, *74*, 493−500.
(35) Liu, R. K.; Hu, T. T.; Jia, J.; Yang, D. L.; Sun, Q.; Wang, J. X.; Chen, J. F. Efficient Fabrication of Polymer Shell Colloidosomes by a Spray Drying Process. *Ind. Eng. Chem. Res.* **2021**, *60*, 324−332.
(36) Liu, R. K.; Gu, Y. H.; Jia, J.; Qiao, M.; Wei, Y.; Sun, Q.; Zhao, H.; Wang, J. X. Three-Fluid Nozzle Spray Drying Strategy for Efficient Fabrication of Functional Colloidosomes. *Langmuir* **2022**, *38*, 16194−16202.
(37) Lin, D.; Liu, Y.; Jia, Z.; Qi, S.; Wu, D. Structural Evolution of Macromolecular Chain during Pre-Imidization Process and Its Effects on Polyimide Film Properties. *J. Phys. Chem. B* **2020**, *124*, 7969−7978.
(38) Pan, R.; Liu, X.; Zhang, A.; Gu, Y. Molecular Simulation on Structure-Property Relationship of Polyimides with Methylene Spacing Groups in Biphenyl Side Chain. *Comput. Mater. Sci.* **2007**, *39*, 887−895.
(39) Mazlan, N.; Jusoh, N.; Sow Mun Lock, S. Investigation of Transport Properties of 6FDA-Durene Polymeric Membrane for Landfill Gas Application Using Molecular Simulation Approach. *Chemosphere* **2022**, *307*, No. 136019.
(40) Abraham, M. J.; Murtola, T.; Schulz, R.; Páll, S.; Smith, J. C.; Hess, B.; Lindahl, E. GROMACS: High Performance Molecular Simulations through Multi-Level Parallelism from Laptops to Supercomputers. *SoftwareX* **2015**, *1*−*2*, 19−25.
(41) Song, X.; Guo, H.; Tao, J.; Zhao, S.; Han, X.; Liu, H. Encapsulation of Single-Walled Carbon Nanotubes with Asymmetric Pyrenyl-Gemini Surfactants. *Chem. Eng. Sci.* **2018**, *187*, 406−414.
(42) Horn, D.; Rieger, J. Organic Nanoparticles in the Aqueous Phase-Theory, Experiment, and Use. *Angew. Chem., Int. Ed.* **2001**, *40*, 4330−4361.
(43) Hu, J.; Lu, C.; Yang, L. Influence of thermal fluctuations on the interactions between nanoscale particles. *J. Nanopart. Res.* **2018**, *20*, 163.
(44) Zoli, M. Twist-Stretch Relations in Nucleic Acids. *Eur. Biophys. J.* **2023**, *52*, 641−650.
(45) Khezri, A.; Karimi, A.; Yazdian, F.; Jokar, M.; Mofradnia, S. R.; Rashedi, H.; Tavakoli, Z. Molecular Dynamic of Curcumin/Chitosan Interaction Using a Computational Molecular Approach: Emphasis on Biofilm Reduction. *Int. J. Biol. Macromol.* **2018**, *114*, 972−978.
(46) Kopera, B. A. F.; Retsch, M. Computing the 3D Radial Distribution Function from Particle Positions: An Advanced Analytic Approach. *Anal. Chem.* **2018**, *90*, 13909−13914.
(47) Schafroth, N.; Arpagaus, C.; Jadhav, U. Y.; Makne, S.; Douroumis, D. Nano and Microparticle Engineering of Water Insoluble Drugs Using a Novel Spray-Drying Process. *Colloid. Surface. B* **2012**, *90*, 8−15.
(48) Sithole, M. N.; Choonara, Y. E.; du Toit, L. C.; Kumar, P.; Marimuthu, T.; Kondiah, P. P. D.; Pillay, V. Development of a Novel Polymeric Nanocomposite Complex for Drugs with Low Bioavailability. *AAPS PharmSciTech* **2018**, *19*, 303−314.
(49) Shamaei, S.; Seiiedlou, S. S.; Aghbashlo, M.; Tsotsas, E.; Kharaghani, A. Microencapsulation of Walnut Oil by Spray Drying: Effects of Wall Material and Drying Conditions on Physicochemical Properties of Microcapsules. *Innov. Food Sci. Emerg.* **2017**, *39*, 101−112.
(50) Zhou, D.; Pan, Y.; Ye, J.; Jia, J.; Ma, J.; Ge, F. Preparation of Walnut Oil Microcapsules Employing Soybean Protein Isolate and Maltodextrin with Enhanced Oxidation Stability of Walnut Oil. *LWT - Food Sci. Technol.* **2017**, *83*, 292−297.

https://doi.org/10.1021/acsomega.3c07802
ACS Omega 2024, 9, 3781−3792